European Journal of Environmental and Civil Engineering

Volume 27 Number 1 January 2023

ISSN: (Print) (Online) Journal homepage: https://www.tandfonline.com/loi/tece20

Mechanical and durability properties of steel, polypropylene and polyamide fiber reinforced slag-based alkali-activated concrete

Ömer Faruk Kuranlı, Mucteba Uysal, Mele Tidjani Abbas, Turgay Çoşgun, Anıl Niş, Yurdakul Aygörmez, Orhan Canpolat & Mukhallad M. Al-mashhadani

To cite this article: Ömer Faruk Kuranlı, Mucteba Uysal, Mele Tidjani Abbas, Turgay Çoşgun, Anıl Niş, Yurdakul Aygörmez, Orhan Canpolat & Mukhallad M. Al-mashhadani (2023) Mechanical and durability properties of steel, polypropylene and polyamide fiber reinforced slag-based alkali-activated concrete, European Journal of Environmental and Civil Engineering, 27:1, 114-139, DOI: 10.1080/19648189.2022.2031302

To link to this article: https://doi.org/10.1080/19648189.2022.2031302

Published online: 03 Feb 2022.

EUROPEAN JOURNAL OF ENVIRONMENTAL AND CIVIL ENGINEERING
2023, VOL. 27, NO. 1, 114–139
https://doi.org/10.1080/19648189.2022.2031302

Mechanical and durability properties of steel, polypropylene and polyamide fiber reinforced slag-based alkali-activated concrete

Ömer Faruk Kuranlı[a], Mucteba Uysal[a], Mele Tidjani Abbas[b], Turgay Çoşgun[b], Anıl Niş[c], Yurdakul Aygörmez[a], Orhan Canpolat[a] and Mukhallad M. Al-mashhadani[c]

[a]Civil Engineering Department, Yildiz Technical University, Istanbul, Turkey; [b]Civil Engineering Department, Istanbul University-Cerrahpasa, Istanbul, Turkey; [c]Civil Engineering Department, Istanbul Gelisim University, Istanbul, Turkey

ABSTRACT

Alkali-activated composites are significant materials in reducing CO2 emissions and ensuring sustainability. With the increasing concerns about climate change globally, the interest in alkali-activated materials has also increased. Researching different fibers has very important potential in this area. This study aims to make alkali-activated concretes widespread in the concrete sector by using the materials common in conventional concretes and ensuring that alkali-activated concretes are an alternative in terms of sustainability. Experimental studies were conducted to examine the mechanical, durability, and microstructural properties (SEM) of slag-based alkali-activated concrete (AASC) reinforced with three various fibers. The fibers, polypropylene (PP), polyamide (PA), and steel (ST), were used with two ratios (%0.4 and %0.8 by vol.). Compressive, splitting tensile, and flexural strength tests were carried out at 28 and 90 days. In terms of durability properties, the samples were exposed to high temperatures (300–600–900 °C) and freeze-thaw test (250 cycles). The results showed that the addition of fibers improved the strength and durability properties; for instance, the existence of steel and polypropylene fibers increased the flexural toughness factor values by 430% and 260%, respectively. Moreover, the compressive strength of the fibrous samples exposed to 900 °C was obtained in the range of 6-23 MPa.

ARTICLE HISTORY
Received 19 August 2021
Accepted 14 January 2022

KEYWORDS
GGBS; alkali-activated concrete; steel fiber; synthetic fibers; high-temperature; freeze-thaw

1. Introduction

Portland Cement is the main ingredient in concrete that binds aggregates together (Shaikh, 2013). However, Ordinary Portland Cement (OPC) production has a tremendous environmental impact, as it causes high greenhouse gas emissions into the atmosphere (Hardjito et al., 2004). A high amount of energy is required during Portland cement production. This situation causes a high amount of CO_2 emission. Cement production is 5% effective in CO_2 emission, which is the leading cause of global warming, and a tonne of cement production emits approximately one ton to the atmosphere (Malhotra and Mehta, 2002). This fact has led to the use and search for new sustainable, less Portland Cement-added

CONTACT Ömer Faruk Kuranlı omerkuranli@icloud.com Civil Engineering Department, Yildiz Technical University, Davutpasa Campus, Istanbul, Turkey.

Supplemental data for this article is available online at at http://doi:10.1080/19648189.2022.2031302.

and cement-supplementary materials (ground granulated blast furnace slag, fly ash) in the concrete industry (Shaikh, 2013).

Alkali activation is the name given to applying a solid aluminosilicate called a precursor to produce a hardened binder under alkaline conditions. Alkali-activated binders (sometimes called geopolymer) have been introduced as a sustainable cement system and can be produced with a wide variety of aluminosilicate precursors (Provis, 2018). In alkali-activated systems, ground granulated blast furnace slag (GGBS) and fly ash can be used together to improve reactivity (Duxson and Provis, 2008). In many studies in the literature, it has been seen that GGBS was used alone in alkali binder systems, and it exhibited superior mechanical and microstructural properties (El-Sayed et al., 2011; Pu et al., 1988). On the other hand, adding fibers (steel, polypropylene, and polyvinyl alcohol fibers) can improve the strength properties of alkali-activated mortar and concrete (Al-Mashhadani et al., 2018). The primary purpose of adding fiber material in concrete or mortar is to direct the brittle fracture to ductile behavior and increase the flexural and tensile strengths.

Timothy et al. (2021) investigated the resistance of fly ash-slag based alkali-activated concrete in aggressive environments. The findings showed that the chloride, freeze-thaw and acid resistance of alkali activated concrete increased as the slag content increased. In the research, it has been revealed that alkali-activated concrete has lower freeze-thaw resistance than concrete with Portland cement. The resistance to surface scaling increased with increasing slag ratio, but it was suggested that more studies should be done to investigate the effect of air entrainment on the freeze-thaw resistance of alkali-activated concretes. In addition, Alkali activated fly ash/slag mixtures had higher acid resistance than Portland cement mixtures. Lower calcium content and silicate-rich gel formation after the calcium aluminum silicate hydrate gel descaled, which reduced further acid ingress and subsequent mass losses.

PP fibers are in the class of synthetic fibers and are produced as a by-product of petroleum refining processes (Hossain et al., 2019). PP fiber is preferred for fiber reinforcement due to its cheapness, stability in alkaline environments, hydrophobic, and high melting point (Noushini et al., 2018). Puertas et al. (2003) studied the mechanical and durability properties of alkali-activated mortars produced with polypropylene fibers. PP fibers were used in the ratios of 0%, 0.5%, and 1% by volume. The compressive strengths of the mortars produced with ground granulated blast furnace slag (GGBS) and 0.5% and 1% PP fibers did not give effective results compared to the control series. Also, the use of PP fiber reduced the flexural strength of GGBS mortars in the study. Nevertheless, PP fiber-reinforced alkali-activated slag mortars exposed to the freeze-thaw effect showed higher resistance than alkali-activated fly ash mortars. Increase after the freeze-thaw effect was attributed to the continuous activation of the slag due to the high humidity environment used in the test (Adesina, 2020). Yurt (2020) investigated the fracture energy of alkali-activated slag concretes produced with various fibers and stated that the use of PP fibers significantly increased the fracture energy compared to concrete produced without fiber. It was seen that PP fibers showed a good adherence in SEM images and were also in a good distribution. Zhou et al. (2021) studied the mechanical properties of alkali-activated concretes with different dosages and lengths of basalt and PP fibers. Researchers stated that the compressive strength increased in the first but then decreased with the increase of fiber ratio. The optimum fiber dosage was suggested as 0.6% by volume in the study.

On the other hand, the use of steel fibers attracts attention in research studies regarding its effect in improving the fracture of concrete and its relatively low cost (Bhutta et al., 2017). While ST fibers are widely used to reinforce conventional concrete, they are produced from cold-drawn wire, sheet metal, and other forms of steel (Al-Majidi et al., 2017). Khalaj et al. (2015) investigated the tensile strength of ST fibered slag-based geopolymer composites in line with the effect of production parameters and evaluation of their optimum conditions. The researchers stated that the splitting tensile strengths were the highest when using 5% fiber reinforcement by weight. Koenig et al. (Koenig et al., 2019) stated that ST fibers could exhibit post-hardening behavior after initial crack load in alkali-activated concretes. It did not affect the compressive strength with the polypropylene and steel fibers used in the study. There was a 13% loss in the compressive strength of alkali-activated binder concretes. This decrease in compressive strength was attributed to the increased voids ratio and viscosity due to the high fiber content. Post-hardening behavior was observed in all concretes with PP fiber. The low modulus of elasticity and high binding behavior of PP fibers were thought to be effective. El-Hassan and Elkholy (2021) investigated the mechanical properties of alkali-activated slag-fly ash mixed concrete containing different hybrid

combinations of steel fibers at a volume fraction of 1%. Experimental results showed that hybridization of steel fibers at a certain dosage resulted in superior mechanical properties compared to fiberless series.

PA fibers represent a potential area for research and application in improving concrete and mortar fracture properties (Celik et al., 2018). However, studies examining the relationship between geopolymer/alkali-activated mortar and concrete with PA fibers are almost negligible in the literature. Celik et al. (2018) investigated the high-temperature behavior and mechanical properties of boron waste additive metakaolin-based geopolymer composites reinforced with polyolefin, basalt, modified polyamide, and polyvinyl alcohol fibers. It has been observed that PA fibers made a significant contribution to the load-displacement values in terms of ultimate load and mid-span deflection values. However, it has been stated that the samples with polyamide fibers, which were exposed to high-temperature effects, experienced more weight loss compared to other fiber-added mortars. Aygörmez et al. (2020) investigated the long and short-term effects of the curing conditions of fiber-reinforced colemanite substituted metakaolin-based geopolymer composites. Polyolefin and PA fibers were used in the ratio of 0.5, 1, and 1.5% by volume. While the highest flexural strength results were obtained using high fiber ratios, polyamide fibers gave higher results than polyolefin fibers due to the stronger bonding degree and higher tensile strength of PA fibers in the geopolymer matrix.

Concrete can be also exposed to high temperatures due to fire or wars. For such dangerous scenarios, concrete must be a material resistant to high temperatures. Factors such as aggregate type, raw material components, binder-alkali ratio, environmental conditions affect the resistance of alkali-activated concrete to high temperature (Turkey et al., 2021). Qu et al. (2020) studied the high-temperature performance of alkali-activated concretes produced with slag/fly ash. In the study, slag was substituted for fly ash. It has been observed that the residual compressive strengths of the alkali-activated concrete exposed to 300 °C, 500 °C, and 700 °C decrease more than the unheated samples with the increase of slag substitution. Rao et al. (2019) studied the effects of different high temperatures (200 °C, 400 °C, 600 °C and 800 °C) on fly ash/slag based alkali-activated concrete. According to the results obtained, the samples exposed to 200 °C gave 40% greater results in compressive strength than the unheated samples. The effect of period exposure time at different temperatures was also reported in the study. It was determined that the average loss in compressive strength of alkali-activated concretes exposed to 800 °C was 59.3%, 65.4% and 68.7%, respectively, in the exposure time (30, 60 and 90 minutes) when compared to the strength at ambient temperature. One of the most important effects of high temperature causes mass and volume changes in the composite (Turkey et al., 2021). Md. Nabi and Sarker (2020) produced slag/fly ash-based alkali-activated mortar by replacing the waste glass with sand. The researchers stated that after exposing the samples to 800 °C, there was a significant increase in the volume of the sand-based mortar, and this situation caused longitudinal and transverse cracks on the surfaces.

This study investigated the mechanical and durability properties of alkali-activated concrete produced by various fibers (polypropylene, polyamide, and steel) and GGBS, which are used without calcining compared to other binder materials and without the need for heat curing. Slag as a mineral additives and fibers, which are widely used in concrete technology, were evaluated within the scope of this study. Considering that these materials are widely used in concrete technology, it is aimed to increase the usability of alkali-activated composites in the construction sector without the need for heat curing and generalize alkali-activated concrete by using these materials; thus it can be an alternative to conventional concrete, especially in terms of sustainability. It is also aimed to standardize alkali-activated concretes by comparing different building codes. In different fiber ratios, mechanical properties such as compressive, splitting tensile and flexural strengths were tested using steel, polypropylene, and polyamide fibers. Non-fibrous and fiber-reinforced alkali-activated slag concretes without air-entraining additives were subjected to freeze-thaw test at 250 cycles and subjected to compressive and flexural tests. Moreover, after non-fibrous and fiber-reinforced alkali-activated slag samples were exposed to 300–600–900°C, ultrasonic pulse velocity, compressive strength, and weight loss results were obtained. Also, SEM analysis has been performed to examine the microstructure properties and to understand the interaction between fibers and matrix.

2. Materials and methods

The testing methodology is described under the following headings. Three specimens were used in all tests for mechanical and durability properties. The values obtained represent the mean value of three samples.

Table 1. Chemical composition of ground blast furnace slag (GGBS).

Oxides	SiO_2	Al_2O_3	Fe_2O_3	CaO	MgO	SO_3	Na_2O	TiO_2	LOI
Amount (%)	40.5	12.8	1.1	35.5	5.8	0.18	0.79	0.75	0.03

2.1. Materials characterization

The ground granulated blast furnace slag used throughout the study was purchased from Bolu Cement Industry. The specific gravity of the slag is 2.91 and its chemical properties are shown in Table 1.

Sodium hydroxide (NaOH) and sodium silicate (Na_2SiO_3) were supplied from As Chemistry Industry and Trade Company. Sodium hydroxide pellets were diluted one day before pouring concrete using distilled water to have a 12 M concentration. The physical and chemical properties of sodium silicate and sodium hydroxide solution are shown in Tables 2 and 3.

Polypropylene fibers were obtained from Kordsa Global Industrial Company and satisfy EN 14990-2 fiber class. Polypropylene fibers have a specific gravity of 0.91 and a fiber length of 54-90 mm. The tensile strength of the fibers is 550 MPa and the melting temperature is about 160 °C. Hooked-end steel fibers supplied from Group Energy Iron and Steel Industry with a thickness of 0.55 mm, a length of 35 mm, a tensile strength of 1100 MPa and a specific gravity of 7.85 were utilized. Polyamide fibers were supplied from Kordsa Global Industrial Company. In light of the information provided by the company, the fibers can absorb moisture by 5%, so they were rubbed with a slightly damp cloth before mixing. Polyamide 6.6 fibers satisfy the EN 14889-2 Class I standard, and it has a specific gravity of 1.14, fiber lengths of 6 and 12 mm, and tensile strength of 900 MPa. Also, all fibers used in the study are shown visually as in Figure 1.

Polycarboxylic ether-based, highly water-reducing superplasticizer MasterGlenium 51 concrete admixture supplied from BASF was used as a superplasticizer. Technical specifications of the plasticizer additive are given in Table 4.

2.2. Experimental methodology

Fibers were added to the AASC in the proportion of 0.4% and 0.8% by volume for each fiber class to inspect the effect of ratios of different fibers on the behavior of AASC under the conducted tests. Suffixes in the mix ID represent steel for ST, polypropylene for PP, and polyamide for PA followed then by the fibers ratio number. Seven mixtures in total were prepared and Table 5 summarizes the mix designs of non-fibrous and fibrous AASC's.

2.3. Mix preparation

Detailed procedures for mixing AASCs are described as follows: In the study, 100 mm side cubes, 100 × 200 mm cylinders, 100 × 100 × 500 mm metal prism molds were used to perform flexural strength, compressive strength, splitting tensile strength, high-temperature, and freeze-thaw tests. Alkali activators were prepared 24 hours before concrete casting. According to the amounts obtained from the mixing design, 12 molars of sodium hydroxide solution was prepared using distilled water. The dry mixture was mixed into the concrete mixer (aggregates to be saturated dry surface) to obtain a homogeneous mixture. Immediately afterward, the alkali activators prepared the day before were poured together with the superplasticizer. After mixing the alkali activators and the dry mixture for two minutes, the mixer was stopped, the fibers (according to the concrete class produced) and additional water were poured and mixed again for two minutes. After the completion, the mixture was poured into cubes, cylinders, and prism molds. The vibration was applied to the casting to evacuate the air gaps and to obtain a homogeneous mixture. To prevent alkali volatility immediately after casting, the top of the molds were covered with plastic covers. After 24 hours, the AASC samples were removed from the molds and cured at room temperature as shown in Figure 2.

Table 2. Physical and chemical properties of sodium silicate.

SiO2	Na2O (%)	Fe (%)	Heavy metals (%)	Density (20 °C) (g/cm^3)	pH
27.0	8.2	≤0.005	≤0.005	1.360	11–12.4

Table 3. Physical and chemical properties of sodium hydroxide.

NaOH (%)	Na_2CO_3 (%)	SO_4 (%)	Cl (%)	Al (%)	Fe (%)	pH	Density (gr/cm^3)	Boiling Point (°C)
99	0.3	≤0.01	≤0.01	≤0.002	≤0.002	14	2.13	1388

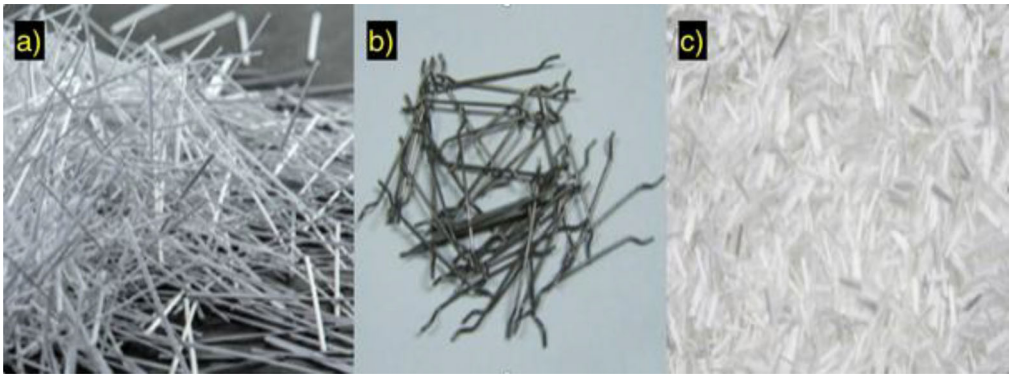

Figure 1. The fibers: (a) polypropylene, (b) steel, and (c) polyamide fibers.

Table 4. Technical specifications for superplasticizer.

Structure of the material	Modified polycarboxylic ether based
Appearance	Brown liquid
Specific gravity (°C)	1.082–1.142 kg/lt
pH	6–7
Alkali content (%)	≤3.0 (by mass)
Chloride content (%)	≤0.10 (by mass)

2.4. Testing

Among the physical property tests, apparent porosity, water absorption, and unit weight values were determined in accordance with the ASTM C20 (ASTM C20-00, 2015). Three samples were tested for each series and the results were expressed as the average. Before the compressive strength test, the ultrasonic pulse velocity test has been carried out for the cube samples after 90 days for the whole mixture series. Ultrasonic pulse velocity test was applied in accordance with the ASTM C597 (ASTM C597, 2016) standard. Compressive and splitting tensile strength tests were carried out after 28 and 90 days. Also, a three-point loading test was carried out for flexural performance in accordance with the ASTM C1609 (ASTM C1609, 2019) standard after 90 days. Shimadzu brand automatic test device with a capacity of 50 kN was used for flexural tests. Flexural toughness values were calculated in accordance with the JSCE-SF4 (JSCE-SF4, 1984) test method.

AASC samples were exposed to 300, 600, and 900 °C in a high-temperature furnace. Nabertherm brand B130 industrial type furnace was used for the high-temperature effect. Before the experiment, the samples were dried in the oven for one day and their weights were measured. The high-temperature effect was applied to all series after 90 days. The device was set on the control panel to increase 5 °C per minute to reach the target temperature and to be kept at the target temperature for 1 hour. The samples were cooled in the oven in order not to be exposed to effects such as explosion and fracture at the end of the test due to possible thermal shock. Some physical and mechanical changes of the samples were analyzed after exposure to heat. The results of compressive strength, weight loss, and ultrasonic pulse velocity were investigated.

After 90 days, AASC samples were subjected to freeze-thaw tests with a total of 250 cycles. Temperature values ranged from −20°C to 20°C, with 12 hours hot and 12 hours cold. In order to

Table 5. Mixture ID notation and concrete composition.

Mixture ID	GGBS (kg/m3)	Fine aggregate (kg/m^3)	Coarse aggregate (kg/m^3)	Type of fibre	Fibre dosage (V%)	Superplasticizer (kg/m^3)	Na_2SiO_3 (kg/m^3)	NaOH (kg/m^3)	Alkali solution/binder
100S (Control)	360	746	1120	–	0	6	115.7	46.3	0.45
100S04PP	360	746	1120	Polypropylene	0.4	6	115.7	46.3	0.45
100S08PP	360	746	1120	Polypropylene	0.8	6	115.7	46.3	0.45
100S04ST	360	746	1120	Steel	0.4	6	115.7	46.3	0.45
100S08ST	360	746	1120	Steel	0.8	6	115.7	46.3	0.45
100S04PA	360	746	1120	Polyamide	0.4	6	115.7	46.3	0.45
100S08PA	360	746	1120	Polyamide	0.8	6	115.7	46.3	0.45

evaluate the weight loss results of samples subjected to freeze-thaw tests, their weight was measured before testing. Compressive and flexural strength results were evaluated. In addition, the samples taken out from the freeze-thaw stage were subjected to the ultrasonic pulse velocity test just before the compressive strength test.

3. Result and discussion

3.1. Physical properties

Unit weight, void ratio, water absorption result values are listed in Table 6. In general, physical properties varied according to the type and ratio of fiber. Compared to the reference sample (100S), samples produced with 0.4% fiber by volume showed improvement and decreased porosity, while samples produced with 0.8% fiber by volume showed an increase. The fibrous series gave better water absorption results than the reference series and showed an overall improvement. The water absorption results were correlated with the voids ratio results, and the relationship is shown in Figure 3.

3.2. Compressive strength results

Compressive strength results at 28 and 90 days are shown in Table 7 and Figure 4. Compared to the control series, it was observed that there was a decrease in compressive strength in most of the fibrous series for both 28 and 90 days. The highest decrease in strength occurred in the polypropylene fiber series, and it was found that it gave up to 40% less strength than the control series on the 28th and 90th days. It was stated in the literature that the increase in the use of polypropylene fiber caused a weakening in the compressive strength characteristics of concrete (Al-Mashhadani et al., 2018; Bhutta et al., 2017). The addition of PP fibers causes poor workability in mixtures, leading to poor compaction. Poor workability and compaction caused a decrease in compressive strength (Amran et al., 2022). Series with polyamide fibers gave a strength result of 9-20% less than the control series.

3.3. Splitting tensile strength results

Tensile strength test was applied to the AASC series on 28th and 90th days. Splitting tensile strength tests were carried out adhering to ASTM C496 standards. Three samples were tested for each AASC series and the mean value of the results was recorded.

Splitting tensile strength results and the rate of change of the strengths of 28 and 90 days compared to the control sample and the results of 28/90 days are shown in Table 8. While it was observed that the splitting tensile strength of AASC specimens at 28 days varied between 2 and 3.1 MPa, these values increased and varied between 2.9 and 3.8 at 90 days strength. Among the series, the highest splitting tensile strength values were obtained in the ST fibered AASC series.

When the relationship between fiber usage ratio by volume and splitting tensile strength was examined, the splitting tensile strengths decreased in almost all series at 28 days. However, it was seen that this decrease in strength was less with the increase in the use of fiber by volume, i.e 100S04PA series lost 31.19% compared to the control sample, while 100S08PA experienced a loss of strength with a rate of 15.25%. According to the 90-days results, the highest splitting tensile strength was seen again in the

Figure 2. AASC samples left to cure at room temperature.

steel fiber reinforced-AASC series. Apart from the steel fiber-reinforced AASC samples, it was seen that the splitting tensile strength decreased compared to the control series. No positive effect of PA and PP fibers was seen on the splitting tensile strength results. It has been observed that the PA fiber-reinforced AASC series gave more strength loss results as the volume of fiber usage rate increased. In the literature for AASC concretes with PA fiber, the results on the splitting tensile strength were almost negligible. Therefore, according to the results of the study, it can be said that PA fibers cannot be effective in improving tensile, toughness and post-crack behaviors of AASC. More studies should be done on the relationship between PA fibers and alkali-activated concrete. Reduction in the splitting tensile strength of PP fiber-reinforced AASC series may be due to the agglomeration of PP fibers causing ineffective bridging in the AASC (Adesina, 2020).

3.4. Compressive strength-splitting tensile strength relations

On the other hand, with extensive studies on OPC-based concrete, the tensile strength can be tested conventionally or estimated by compressive strength (Ding et al., 2016). The American Concrete Institute ACI structure code 318 (ACI Committee, 2005) offers the possibility to estimate the splitting tensile strength by using the compressive strength of the corresponding sample. ACI 318 approach is applied to understand the consistency of AASC samples with codes. Splitting tensile strength can be calculated using equation (1) where f_{ct} is splitting tensile strength and $f_c^{'}$ is the compressive strength.

$$f_{ct} = 0.56\sqrt{f_c'} \tag{1}$$

Figure 5 shows the splitting tensile strength and compressive strength relation based on experimental data and ACI 318 structure code. In addition, the proportionality of these results to each other is shown in Table 9. It was seen that the splitting tensile strength of AASC specimens changed marginally with compressive strength and the ACI318 building code had a poor consistency with experimental results. AASC specimens had a linear relationship between the splitting tensile strengths and the experimental's square roots of compressive strengths. Based on the results, the following estimation equation 2 was proposed for the splitting tensile strength of AAS concretes.

$$f_{ct} = 0.42\sqrt{f_c'} \tag{2}$$

More work should be done to establish a general relationship between the compressive strength and the splitting tensile strength of fibrous AAS concrete. There were differences between the equations proposed by researchers in studies. Some previous studies (Chi, 2012; Yang et al., 2012) for AASC have shown highly consistent results with ACI structure code 318. Different equations were proposed in studies where the ACI structure code and AASC experimental studies were inconsistent. Aliebdo et al. (2019) concluded that the splitting tensile strength was 0.5554 times the square root of the average

Table 6. Physical properties of AASC's.

Mix ID	Unit Weight (g/cm^3)	Porosity (%)	Water absorption (%)	Water absorption change (%)	Porosity change (%)
100S	2.59	8.87	3.76	Control	Control
100S04ST	2.61	8.53	3.57	−5.1	−3.8
100S08ST	2.81	9.44	3.71	−1.3	6.4
100S04PP	2.57	7.76	3.27	−13.0	−12.5
100S08PP	2.54	8.5	3.66	−2.7	−4.2
100S04PA	2.57	8.04	3.41	−9.3	−9.4
100S08PA	2.55	9.37	4.05	7.7	5.6

compressive strength, while Parthiban and Mohan (2017) concluded that it was 0.62 times which was not similar to that proposed in this study.

3.5. Flexural strength

Flexural strength results at 90 days are shown in Figure 6. Three-point loading was applied by load from the midpoint of the upper surface of AASC specimens. The improvement ratio in flexural strength of the fiber reinforcement except ST fiber was adversely affected compared to the control sample. It was observed that the improvement rate developed negatively as the amount of fiber usage by volume increased. For instance, sample 100S04ST gained 4.12% strength, while this ratio resulted in 4.2% strength loss in sample 100S08ST. Likewise, while sample 100S04PP showed 6.69% strength loss, this rate increased up to 17.19% in sample 100S08PP. The same evaluation can be made for the AASC series with PA fibers. With the increase in PP fiber dosage amount, the workability of AASC mixtures decreased and as a result, the mixtures cannot be appropriately compacted, causing a reduction in flexural strength (Adesina, 2020).

Displacement controlled flexural test was applied to the AASC series. The load-displacement graph is shown in Figure 7. Series with PP fiber exhibited high displacement property among all series and continued to develop the flexural strength by showing the effect of fiber property after the first crack value, and by increasing the displacement. For example, sample 100S08PP showed the best load-displacement behavior among the series, increasing from the initial crack value of 0.619 mm and 4000 N to 5500 N and again to 4000 N, showing a displacement performance of approximately 7.4 mm. It can be said that short-term ups and downs were effective in load values together with the increase in the displacement value in the PP fibered series and PP fibers positively affected the energy absorption capacity. Also, it was seen that the increase in the use of fiber by volume in the PP fibered series had a positive effect on the development of the flexural strength-displacement graph. Among the steel fiber series, only the 100S08ST series showed outstanding flexural improvement performance compared to the control series. It turned out that the series with 0.4% steel fiber by volume was negligible in improving the flexural performance. It can be said that the increase in the use of steel fiber in the AASC series had a positive effect on the development of load-displacement. Farhan et al. (2018) investigated the effect of different types of steel fibers on the engineering properties of ambient cured, alkali-activated slag-fly ash concrete. In the study, it was determined that the compressive, splitting tensile and flexural strength of slag-fly ash concrete mixtures activated with alkali increased with the addition of steel fibers. Researchers have reported the stress-strain response of concrete mixtures to change from brittle to ductile with the addition of steel fibers.

All of the PA fibered series could not show an increase in flexural strength after the first crack value. Although there were improvements in the displacement value after the displacement value read in the first crack value in the PA fibered series, the small fluctuations in the flexural strength could not exceed the first crack strength value. However, it can be observed that high volume PA fiber series increased the energy absorption capacity compared to the fiberless series.

3.5.1. Relationship between compressive and flexural strength

In conventional concrete technology, flexural strength (f_r) can be estimated by using compressive strength (f_c). ACI Committee 363 (ACI Committee 363, 1997) and IS:456-2000 (IS 456-2000, XXXX) standards define the relationship between compressive strength and flexural strength, respectively, as follows:

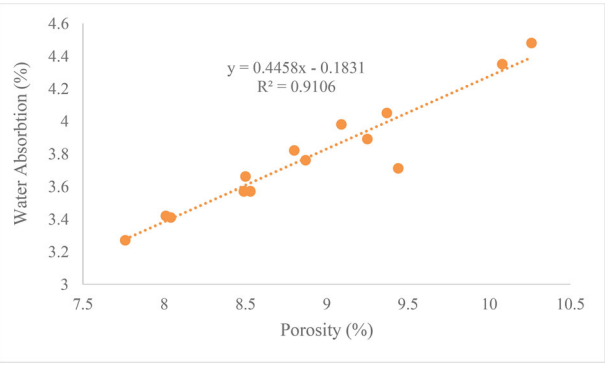

Figure 3. Correlation between porosity and water absorption in AASC.

Table 7. Compressive strength results at 28 and 90 days.

Mix ID	28 Days (MPa)	IR(%)	90 Days (MPa)	IR (%)	28/90
100S	67.49	Control	76.75	Control	0.88
100S04ST	67	−0.73	73.93	−3.67	0.91
100S08ST	58.36	−13.53	79.86	4.05	0.73
100S04PP	51.45	−23.77	65.29	−14.93	0.79
100S08PP	42.17	−37.52	45.41	−40.83	0.93
100S04PA	56.83	−15.79	61.17	−20.30	0.93
100S08PA	53.55	−20.65	61.01	−20.51	0.88

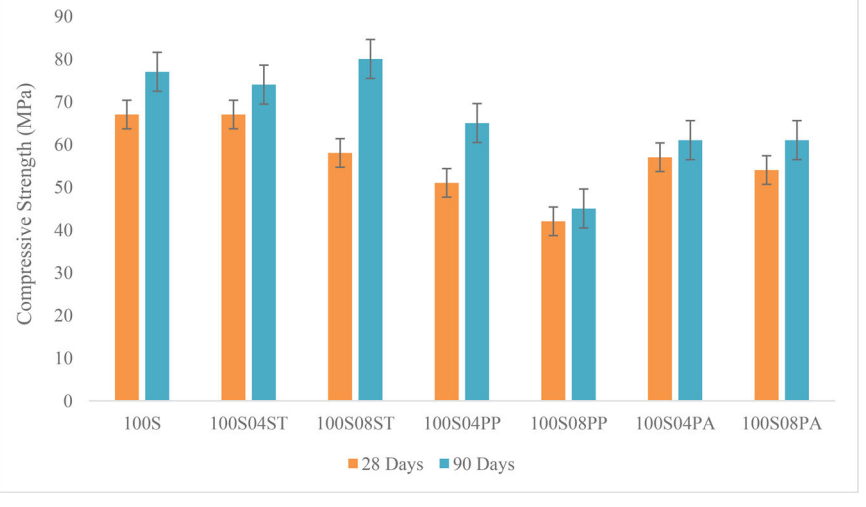

Figure 4. Compressive strength values of the investigated AASC.

Table 8. Splitting tensile strength results at 28 and 90 days.

Mix ID	28 Days (MPa)	IR (%)	90 Days (Mpa)	IR (%)	28/90
100S	2.95	Ref.	3.23	Ref.	0.91
100S04ST	2.75	−6.78	3.22	−0.31	0.85
100S08ST	3.18	7.80	3.85	19.20	0.83
100S04PP	2.15	−27.12	2.93	−9.29	0.73
100S08PP	2.77	−6.10	2.93	−9.29	0.95
100S04PA	2.03	−31.19	2.92	−9.60	0.70
100S08PA	2.50	−15.25	2.78	−13.93	0.90

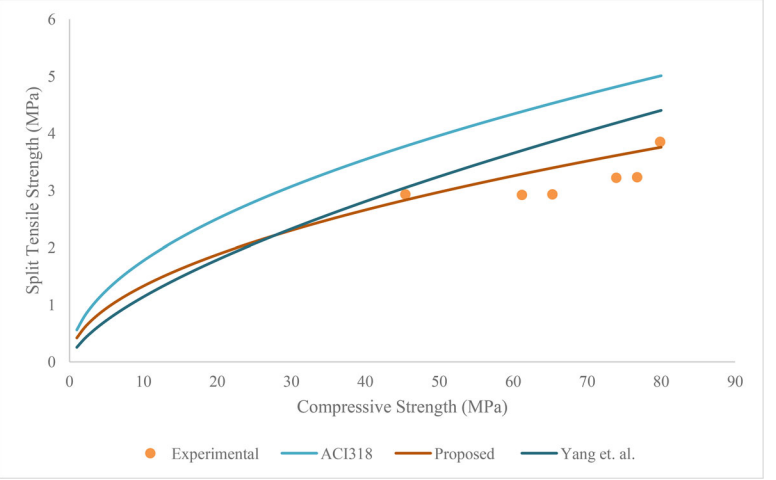

Figure 5. Splitting tensile strength and compressive strength relation.

$$f_r = 0.94\sqrt{f_c} \tag{3}$$

$$f_r = 0.7\sqrt{f_c} \tag{4}$$

Table 10 and Figure 8 shows the results of the estimated flexural strengths and experimental flexural strengths obtained with the models suggested by the mentioned standards. It has been revealed that the ACI Committee 363 standard overestimates the experimental flexural strength values. On the contrary, the IS:456-2000 standard underestimated the actual values. However, it is possible to say that both standards make estimations close to real values. In order to provide more consistent results for FRAAC, a linear relationship with the square root of compressive strength has been revealed and a new equation as follows with a proportionality constant of 0.80 is proposed:

$$f_r = 0.8\sqrt{f_c} \tag{4}$$

3.6. Flexural toughness factor

In order to emphasize the effect of fiber reinforcement on energy under an external load effect of the AASC series, the flexural toughness factor was calculated by applying the JSCE-SF4 (JSCE-SF4, 1984) test. The flexural toughness factor is shown in Figure 9. According to the data obtained from the AASC series, it was revealed that fiber addition gave better results in terms of flexural behavior than the fiberless series. Especially, the ST and PP fibered series with 0.8% by volume showed a quite remarkable toughening effect. For example, while the ST fibered series showed a remarkable increase in flexural factor values from 25% to 430%, in the PP fibered series the values in the two fiber volume classes converged and showed a significant increase of 260% compared to the fiberless series. The results obtained were in accordance with other studies in the literature (Al-Mashhadani et al., 2018; Xu et al., 2017).

3.7. Elevated-temperature test

AASC samples were exposed to high temperatures at 300°C, 600°C, and 900°C. After the tests were completed, weight loss, ultrasonic pulse velocity, and compressive strength tests were performed in each temperature class.

3.7.1. Compressive Strength

Residual strengths and compressive strength loss rates due to elevated temperature tests are shown in Table 11 and Figure 10, respectively. The residual strengths of the fiber-reinforced AASC series at 300 °C

Table 9. Split tensile strength by ACI318 and experimental.

Mix ID	ACI 318 Code	Experimental STS	ACI318/Exp. STS
100S	4.91	3.23	0.66
100S04ST	4.82	3.22	0.67
100S08ST	5	3.85	0.77
100S04PP	4.52	2.93	0.65
100S08PP	3.77	2.93	0.78
100S04PA	4.38	2.92	0.67
100S08PA	4.37	2.78	0.64

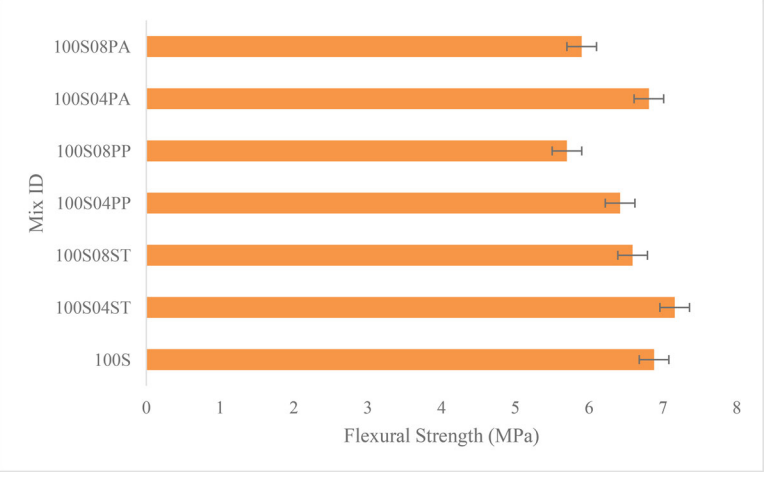

Figure 6. Flexural strength values of investigated mixes.

almost entirely increased compared to the 90-day strength. Similar results were available for fiberless AASC samples in the literature (Fan et al., 2018). These increases in compressive strength were attributed to the low diffusion coefficient of Na^{+}. The low diffusion property resulted in the high melting temperature of AASC. These increases in compressive strength showed that the alkaline activation process continued up to 300–400°C (Hussin et al., 2015). Guerrieri et al. (2009) also explained this by hydration and sintering of unreacted binders. Significant increases occurred in polypropylene and polyamide fiber-reinforced AASC series in 300°C. For example, in the AASC series with 0.4% and 0.8% polypropylene fiber by volume, there was an increase of 49% and 89%, respectively. Likewise, increases such as 30% to 60% were recorded for series with polyamide fiber. The positive behavior of the fibers in the compressive strength up to 300°C can be explained by the large connection in the matrix. Microscopic cracks in the composite tissue can be prevented from turning into macroscopic cracks due to the fibers (Shehab et al., 2016). PP and PA fibers melt at 160–170 and 260°C, respectively. PP and PA fibers melt and create a free path to escape water vapor to release pore pressure (Aygörmez et al., 2020). Kalifa et al. (2001) suggested that the matrix absorbed the molten polypropylene and played a role in the empty fiber beds and pressure relief.

On the other hand, it was seen that there was a serious decrease in the residual compressive strengths at 600°C and 900°C. For a temperature of 600°C, it can be said that there were satisfactory values in terms of compressive strength, although it was seen that there were high losses in the residual compressive strength compared to 90 days. Residual compressive strength at 600 °C varied between 39 and 61 MPa and an average compressive strength of 50 MPa was obtained. It was seen that the highest residual strength at 600 °C was in the steel fiber series. At 600 °C, the losses of AASFC series compared to the 90-day strength were between 8% and 39% and were recorded as an average loss of 32%. It was observed that the compressive strength of the series experienced a significant strength loss at 900 °C. As well as these losses were up to 90%, an average loss of 85% occurred in all series. Compressive strength at 900 °C varied between 6 and 23 MPa. Series at 900 °C did not give a satisfactory strength result. It stood out as a result of the residual compressive strength of 23 MPa obtained in the polypropylene fibered series (100S04PP) at 900 °C temperature. It can be said that the voids formed by the release of

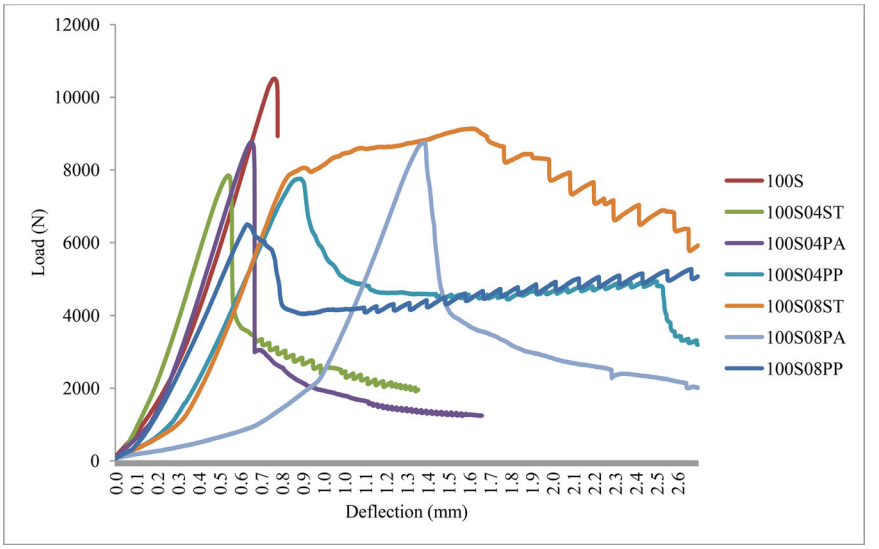

Figure 7. Load-deflection curves of AASC.

free water from the mass due to the high-temperature effect, the polypropylene fibers melted and were effective in these voids and therefore exhibited higher compressive strength than expected (Aygörmez et al., 2020). Kong et al. (2008) stated that there was an incompatibility between the matrix of high-temperature alkali activated concrete and the expansion of the coarse aggregate. Researchers stated that the matrix shrank by 1% at a temperature of 800 °C, while a certain amount of aggregate expanded up to 2.5%, and the loss of strength was observed in AASC at higher temperatures. It was also stated that replacing amorphous structures in alkali activation by crystalline Na-feldspars at temperatures of 800 °C and above caused a decrease in compressive strength (Mustafa et al., 2011).

3.7.2. Weight loss

Weight loss results in each series after high-temperature tests are shown in Figure 11. At 300 °C, the AASC series lost 5.3% weight on average, and the weight loss ranged from 3.87% to 6.98%. At 600 °C, the weight loss of the series was 6% on average, and the weight loss varied between 4.64% and 7.29%. While the average weight loss was 10% at 900 °C, these values varied between 9.41% and 12.8%. It can be said that the use of fiber had no serious effect on weight loss. Generally, it was seen that the weight loss percentage increased as the temperature increased. An increase in temperature caused dehydration in alkaline activation. The AASC matrix was seriously damaged due to the high-temperature effect, and as a result, the cracks in the concrete expanded even more. It increased the loss of compressive strength by creating matrix voids in expanding cracks. As the temperature rose, dehydration began and moisture escaped by moving towards the sample surface. This led to internal damage of the microstructure and natural weight loss of the composite (Aygörmez et al., 2020).

3.7.3. Comparison of experimental results with existing models

The residual compressive strength at high temperatures can be estimated by many empirical models. The empirical models (Equations (5)–(8)) in the literature and the Eurocode (2005) standard are shown below:

$$f'_{cT} = \mu * f'_c \text{ by Eurocode} \tag{5}$$

$$f'_{cT} = f'_c \left\{ 1 + \frac{T}{1000} - 2*\left(\frac{T}{1000}\right)^2 \right\} \ (100\ ^\circ\text{C} \le T \le 800\ ^\circ\text{C}) \text{ by Shaikh and Hosan (2016)} \tag{6}$$

Table 10. Experimental and theoretical results of flexural strengths.

Mix ID	Experimental f_r (MPa)	f_r by ACI Committee 363	ACI Com. 363/Experimental	f_r by IS:456-2000	IS:456-2000/ Experimental
100S	6.88	8.24	1.20	6.13	0.89
100S04ST	7.16	8.08	1.13	6.02	0.84
100S08ST	6.59	8.40	1.27	6.26	0.95
100S04PP	6.42	7.60	1.18	5.66	0.88
100S08PP	5.70	6.33	1.11	4.72	0.83
100S04PA	6.81	7.35	1.08	5.47	0.80
100S08PA	5.90	7.34	1.24	5.47	0.93

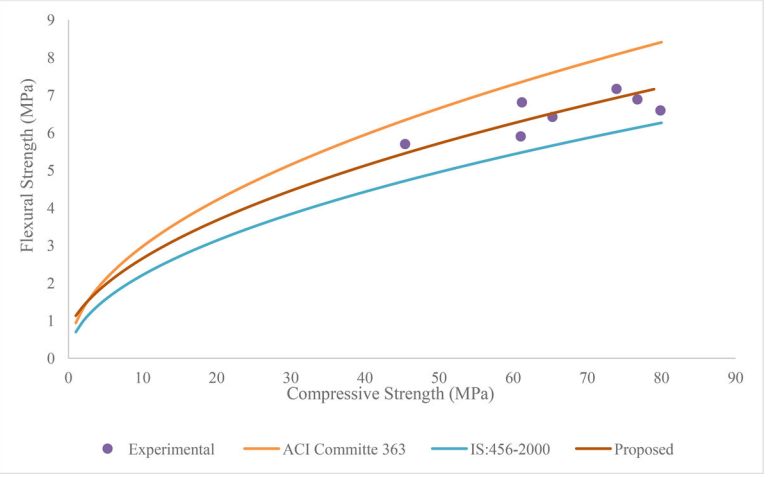

Figure 8. Comparison between predicted flexural strength and experimental flexural strength of FRAAC samples.

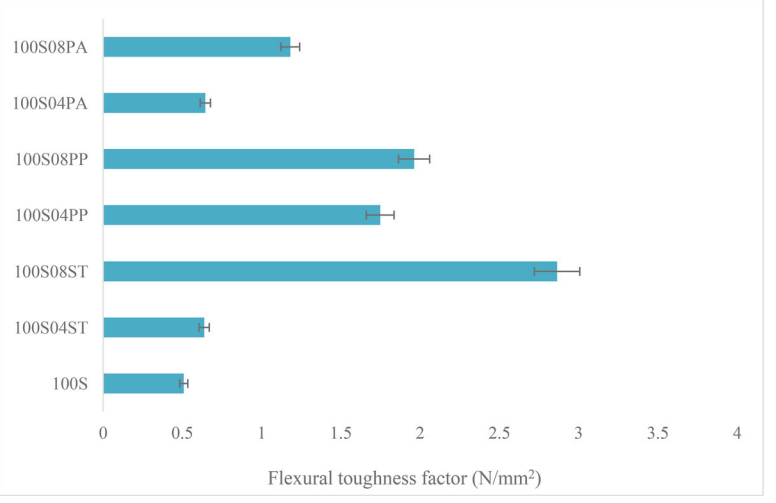

Figure 9. Flexural toughness factor of investigated series.

$$f'_{cT} = f'_c \begin{cases} 0.93 + 0.0025T - 7x10^{-6}T^2 & 100°C \le T \le 400°C \\ 1.0242 + 0.0006T - 2x10^{-6}T^2 & 400°C \le T \le 800°C \\ 1.0252 - 0.001T + 2x10^{-7}T^2 & 600°C \le T \le 1200°C \end{cases} \text{ by Aslani and Samali (2014)} \quad (7)$$

$$f'_{cT} = 1.268 * e^{-\left(\frac{T-259.7}{532.8}\right)^2} * f'_c \text{ Zhang et al. (2020).} \quad (8)$$

Table 11. Compressive strength loss retes after elevated temperature.

Mix ID	300°C (%)	600°C (%)	900°C (%)
100S	0.00	−38.96	−90.91
100S04ST	+16.22	−22.97	−87.84
100S08ST	+6.25	−23.75	−92.50
100S04PP	+49.23	−18.46	−64.62
100S08PP	+88.89	−8.89	−75.56
100S04PA	+60.66	−13.11	−83.61
100S08PA	+39.34	−36.07	−75.41

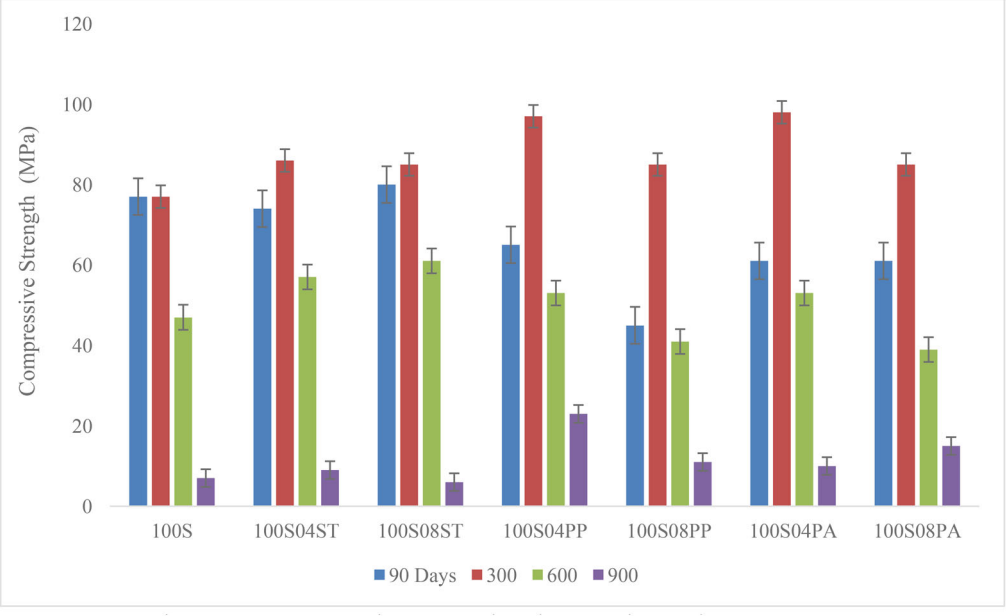

Figure 10. Compressive strength values at elevated temperatures.

where f'_{cT} is predicted residual compressive strength at elevated temperature (MPa), T is elevated temperature in °C, f'_c is compressive strength at ambient temperature, e is natural constant, μ is reduction factor recommended by Eurocode.

Figures 12–18 show the comparison of the estimated compressive strength values obtained with the empirical models mentioned and the measured compressive strength values. It has been revealed that the estimated compressive strength values obtained for 300 °C temperature give lower results than the experimental compressive strength values in almost all empirical models. The models recommended by Zhang et al. and Eurocode at 300 °C showed relatively more consistent results compared to other models. At the estimated compressive strengths obtained at 600 °C, all the models proposed showed much more consistent results than the estimated compressive strengths obtained at 300 and 900 °C. In general, the Eurocode model gives closer results than other recommended models. It has been seen that the estimated compressive strengths obtained by Eurocode at 900 °C are quite compatible with the measured compressive strength values. More studies need to be done to confirm the consistency of existing models.

3.8. Freeze-thaw test

Freezing and thawing are essential parameters for underwater structures in cold regions and are an evaluation criterion for concrete durability. Figure 19 shows the compressive strengths of AASC before and after 250 cycles. Also, Tablo 12 shows the improvement rates of the residual compressive strengths according to the 90-day compressive strengths.

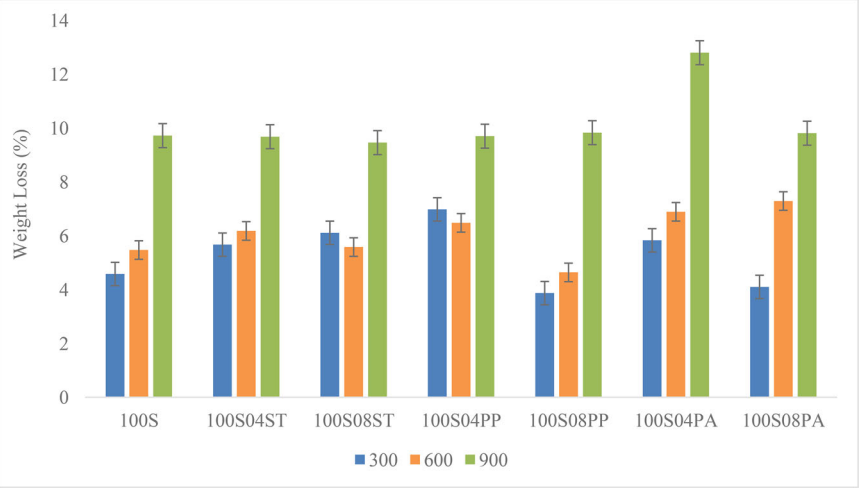

Figure 11. Weight loss of each series as a result of elevated temperatures.

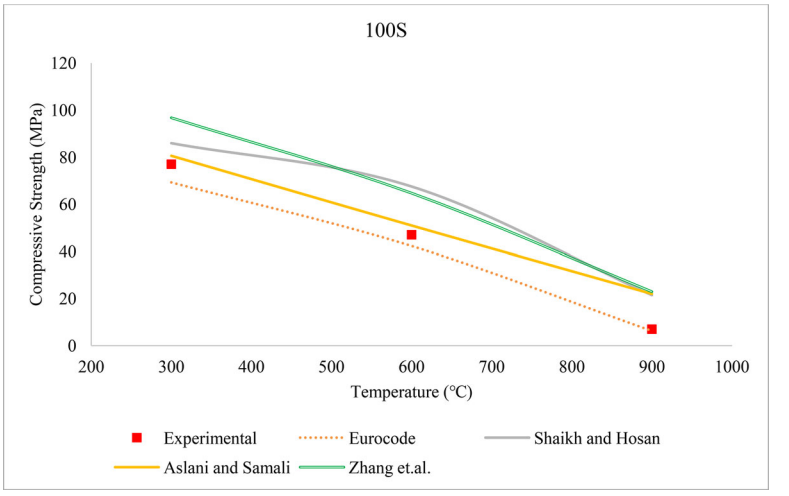

Figure 12. Comparison of experimentally measured compressive strengths of 100S with existing models.

As seen in Table 11 and Figure 11, one of the most significant results of AASC samples after being exposed to the freeze-thaw effect was the increase in residual compressive strength in some mixture classes. These increases ranged from 2.3% to 11.9%. Increases in residual compressive strength revealed that the GGBS binder continued to activate alkali under high humidity conditions during the freezing-thawing tests. Activation produced a large amount of reaction product, improving the residual strengths (Puertas et al., 2003). The humid environment allowed the gaps to be filled with the reaction products of the binder. Due to the compactness of the alkaline activation matrix and its good adhesion, the samples became resistant to the freezing-thawing effect (Aygörmez et al., 2020). The process of development of the residual strengths can be considered as a continuation of the curing process in alkaline activation (Kampala et al., 2014). It was seen that PA fibered mixes had the best improvement rate in the residual compressive strengths. The increase in the use of PA fibers had a positive effect on the development of residual compressive strength. Using 0.4% PA fiber by volume provided an increase of 8% while using 0.8% by volume fiber provided an increase of approximately 12%. No improvement was observed in the residual compressive strengths with the use of PP fiber. The loss in remaining strength decreased with the increase in PP fiber usage. The increase in the use of ST fiber negatively affected the development of

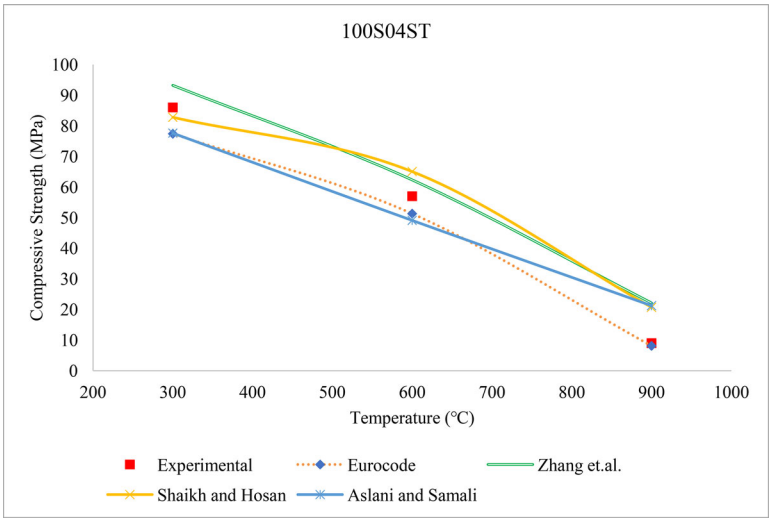

Figure 13. Comparison of experimentally measured compressive strengths of 100S04ST with existing models.

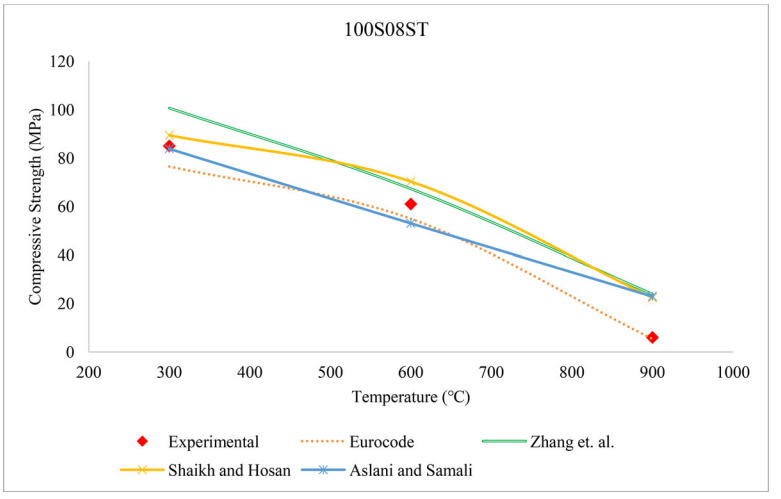

Figure 14. Comparison of experimentally measured compressive strengths of 100S08ST with existing models.

residual compressive strength. The doubling of the use of ST fiber in volume decreased compressive strength by 2.1% compared to the 90-day strength.

It was seen that the use of fiber did not have a positive effect on residual compressive strength after 250 freeze-thaw cycles when compared to the control sample which was a fiberless series as seen in Figure 11. According to the results of freeze-thaw tests, the PP fiber reinforcement for AASC samples affected the results most negatively. PP fibers resulted in an average of 36% loss of compressive strength compared to the fiberless series, and it was observed that this loss increased as fiber usage increased. Likewise, the increase in the use of ST fiber by volume also adversely affected the development compared to the control series. In the PA fibered series, this situation was the opposite; as the fiber usage volume increased, the rate of decrease in the residual compressive strength decreased. However, it was found that PA fibers also did not improve compressive strength in general compared to the control series. The only improvement in the residual compressive strength compared to the non-fibrous series after 250 cycles were in the 0.4% ST fiber series with an improvement rate of 2%.

On the other hand, UPV is a non-destructive test method used to identify matrix uniformity and internal cracks. Figure 20 shows the correlation between the residual compressive strengths and UPV

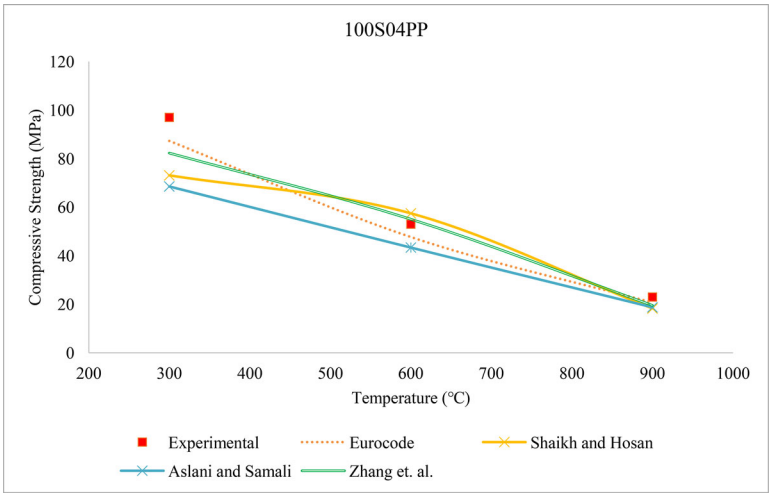

Figure 15. Comparison of experimentally measured compressive strengths of 100S04PP with existing models.

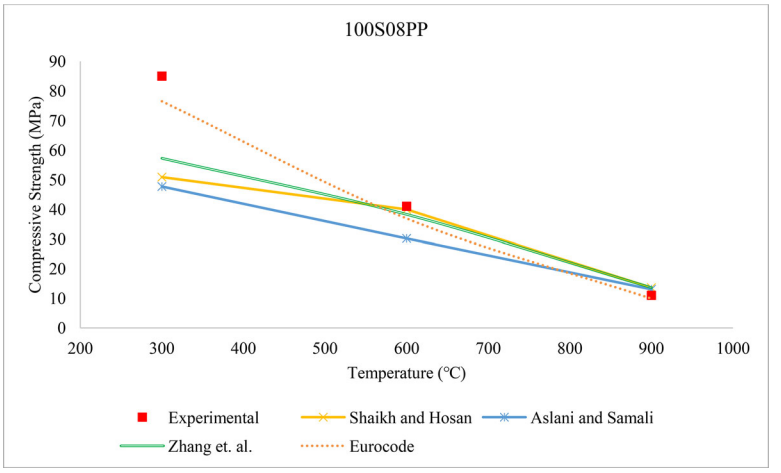

Figure 16. Comparison of experimentally measured compressive strengths of 100S08PP with existing models.

results of the fibrous and non-fibrous series. After 250 cycles of freeze-thaw tests, it was found that the residual compressive strengths and UPV values had an agreeable relationship. The average correlation coefficient of 0.84 showed consistency (Table 12).

Figure 21 and Table 13 show the flexural strength results obtained after 250 cycles of freeze-thaw tests. While the highest flexural strength was 9.83 MPa with the 100S08PA series, the lowest flexural strength result was 6.66 MPa with the 100S08ST series. On the other hand, the samples generally showed an improvement compared to the 90-day flexural strength results. After 250-cycle freeze-thaw tests, it was seen that all series had an average growth rate of 24% compared to 90-day flexural strength. The AASC series that showed minor improvement compared to their 90-day flexural strength were ST fibered series. As the use of ST fibers by volume increased, this growth rate changed from negative to positive. It was seen that the highest growth rate was in series with PA fibers. With the doubling of the PA fiber ratio, it was observed that the improvement in flexural strength almost doubled. The same expressions can be said for the AASC series with PP fiber. Especially, the increase in the use of fiber by volume significantly increased the rate of development five times.

Also, growth rates of the flexural strengths obtained after the freeze-thaw tests were compared to the fiberless control series. Apart from the PA fibered series, it can be said that the fiber addition did not

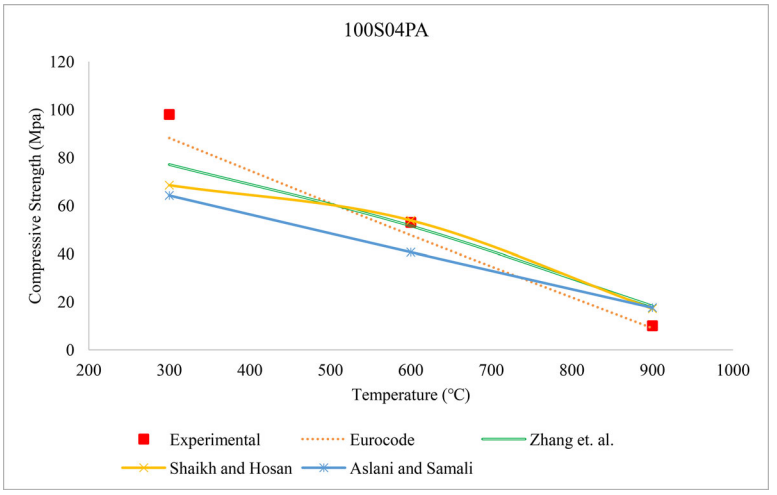

Figure 17. Comparison of experimentally measured compressive strengths of 100S04PA with existing models.

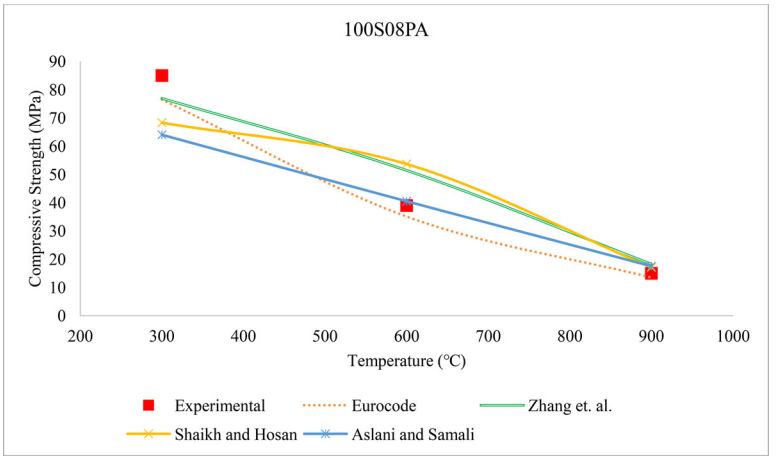

Figure 18. Comparison of experimentally measured compressive strengths of 100S08PA with existing models.

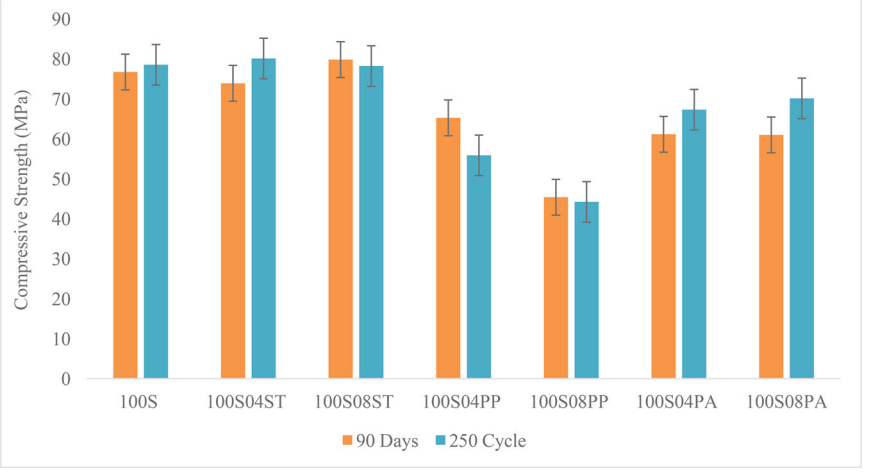

Figure 19. Residual strength results after the freeze-thaw test.

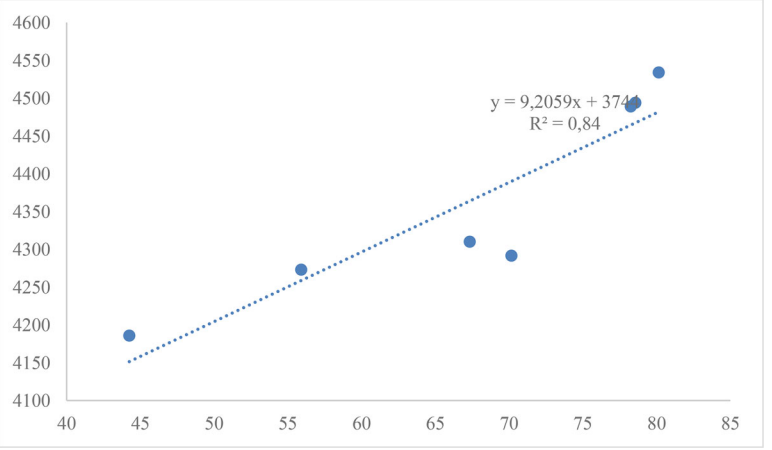

Figure 20. UPV results of AASC's after freeze-thaw tests.

Table 12. Improvement ratio of residual compressive strength.

Mix ID	90 Days (Mpa)	Residual strength, 250 cycle (Mpa)	IR (%)
100S	76.75	78.56	2.36
100S04ST	73.93	80.15	8.10
100S08ST	79.86	78.25	−2.10
100S04PP	65.29	55.90	−12.23
100S08PP	45.41	44.25	−1.52
100S04PA	61.17	67.33	8.03
100S08PA	61.01	70.16	11.92

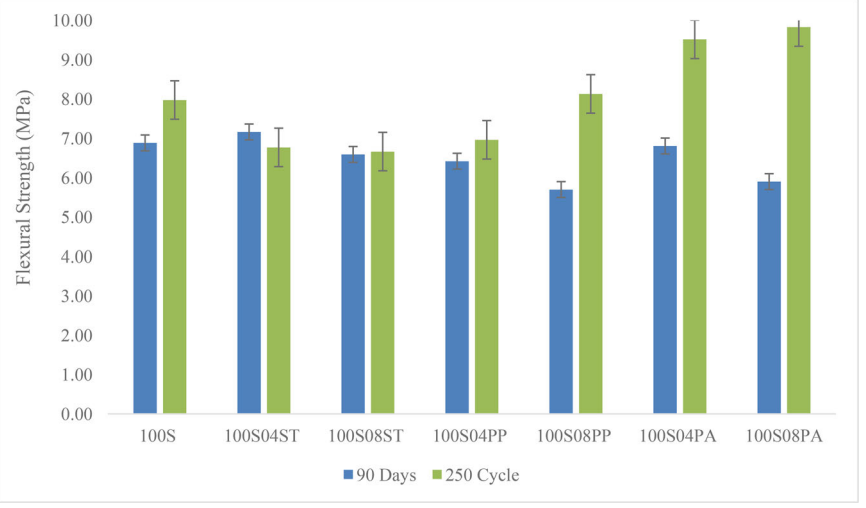

Figure 21. Flexural strength results after freeze-thaw tests.

have a positive effect on the flexural strength results after the freeze-thaw test. While the ST fibered series experienced a 15% loss compared to the control series, the PP fibered series showed slight improvement with the increase in fiber volume. The PA fibered series showed complete improvement compared to the control series. It was seen that PA fiber-reinforced AASC showed an average improvement of 21% compared to the control series and were resistant to the freeze-thaw.

Weight change rates obtained from the freeze-thaw tests are shown in Figure 22. After the freeze-thaw tests, the weight of the samples increased by a small percentage. In the freeze-thaw tests, the filling of the voids in the produced samples by the humidity in the environment caused the weight of the samples to

Table 13. Improvement ratio of residual flexural strength by 90 days and control sample after the freezing-thawing test.

Mix ID	90 Days (MPa)	250 Cylce (MPa)	IR by 90 days (%)	IR by control sample (%)
100S	6.88	7.98	15.84	Control
100S04ST	7.16	6.77	−5.49	−15.11
100S08ST	6.59	6.66	1.10	−16.44
100S04PP	6.42	6.96	8.45	−12.70
100S08PP	5.70	8.13	42.69	1.94
100S04PA	6.81	9.52	39.83	19.34
100S08PA	5.90	9.83	66.61	23.27

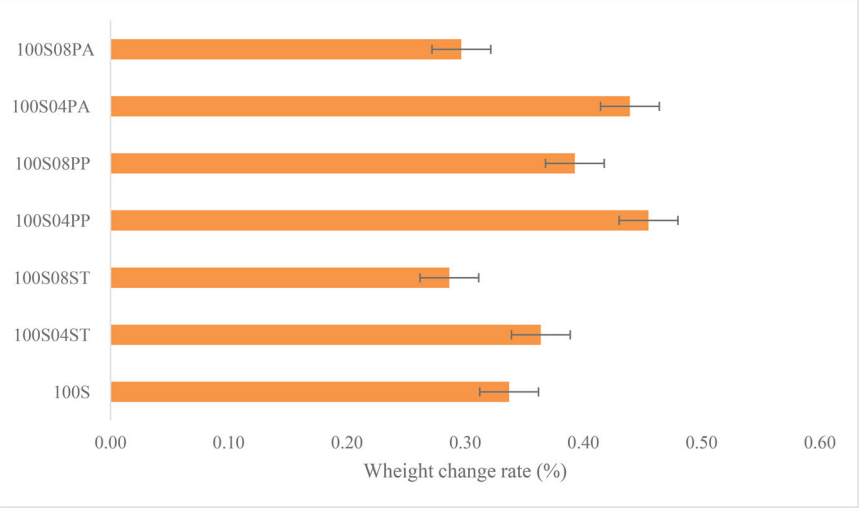

Figure 22. Weight change after the freeze-thaw tests.

increase after 250 cycles (Sun and Wu, 2013). The weight changes that occurred after the freeze-thaw tests were due to the micro-cracks in the samples and the ability of moisture to move into the sample. At the same time, there was a change in weight due to the moisture in the sample moving out. The degraded areas that occurred with the formation of micro-cracks can be filled with the effect of the moist environment and the sample weight can increase (Aygörmez et al., 2020). Awoyera et al. (Awoyera and Adesina, 2020) investigated the durability properties of alkali-activated slag composites. The study revealed that the composites exposed to freezing and thawing showed some scaling after only 40 cycles but did not show any scaling in the same number of cycles in the other mixtures without air entrainment.

3.9. SEM analysis

SEM micrographs of non-fibrous and reinforced AASC specimens are shown in Figures 23–26. In order to understand the microstructural changes of AASC mixtures, SEM analyzes were performed for each mixture class after elevated temperature, freeze-thaw, and mechanical tests. SEM analyses were taken from the fracture AASC samples' core and performed on very tiny samples.

When the SEM images were examined, it was seen that the mixtures were more intense at room temperature and after freezing-thawing in all mixture classes. Unreacted GGBS particles were also seen in micrographs at room temperature. Unreacted GGBS particles can be positively associated with increased compressive strength up to 300°C. While the temperature increase up to 600°C caused cracks in some mixtures, minor changes were observed in the matrix properties in general. However, it turned out that large cracks were formed that became much more visible in all mixture classes after exposure to 900°C. The deterioration in the binder phase, together with the development of micro and macro cracks, caused a decrease in compressive strength and an increase in mass losses with the increase of temperature in almost all mixture classes (Rovnanik et al., 2013). The microstructure of GGBS based AACs became more porous when exposed to high temperatures after 600°C due to matrix decomposition and weight loss.

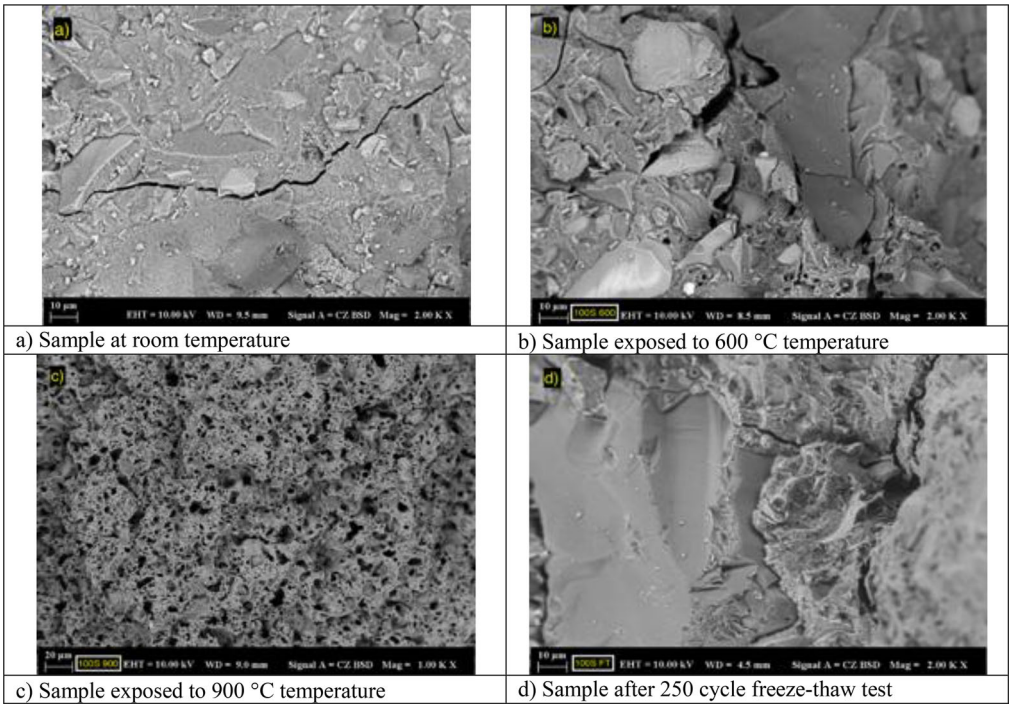

a) Sample at room temperature | b) Sample exposed to 600 °C temperature

c) Sample exposed to 900 °C temperature | d) Sample after 250 cycle freeze-thaw test

Figure 23. SEM micrographs of non-fibrous 100S mix.

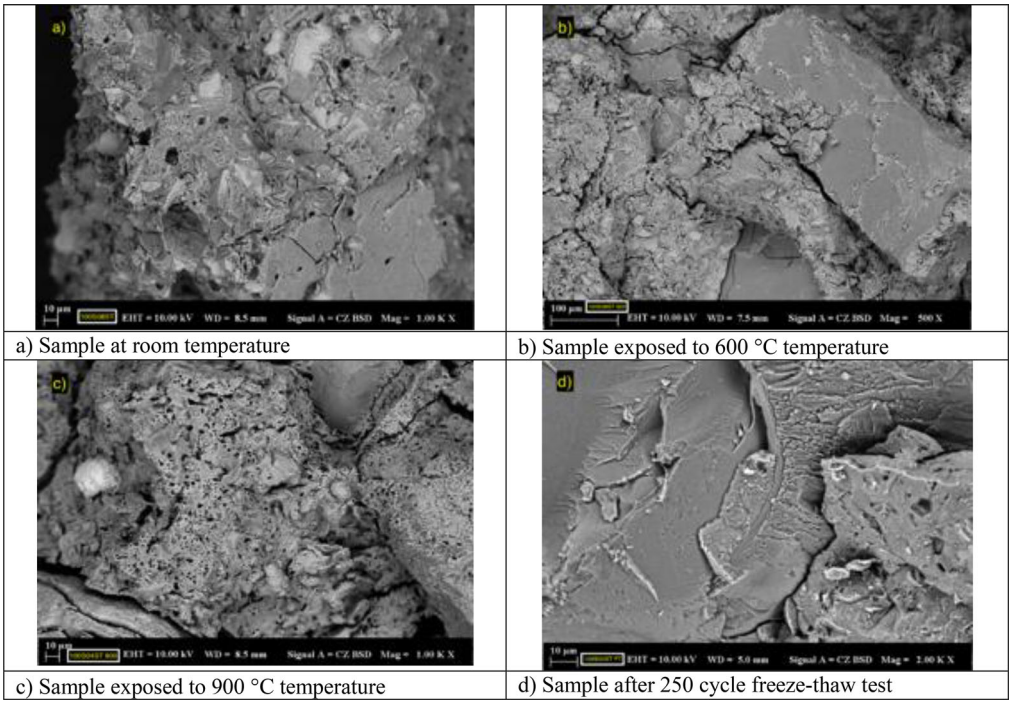

a) Sample at room temperature | b) Sample exposed to 600 °C temperature

c) Sample exposed to 900 °C temperature | d) Sample after 250 cycle freeze-thaw test

Figure 24. SEM micrographs of samples reinforced with ST fibers.

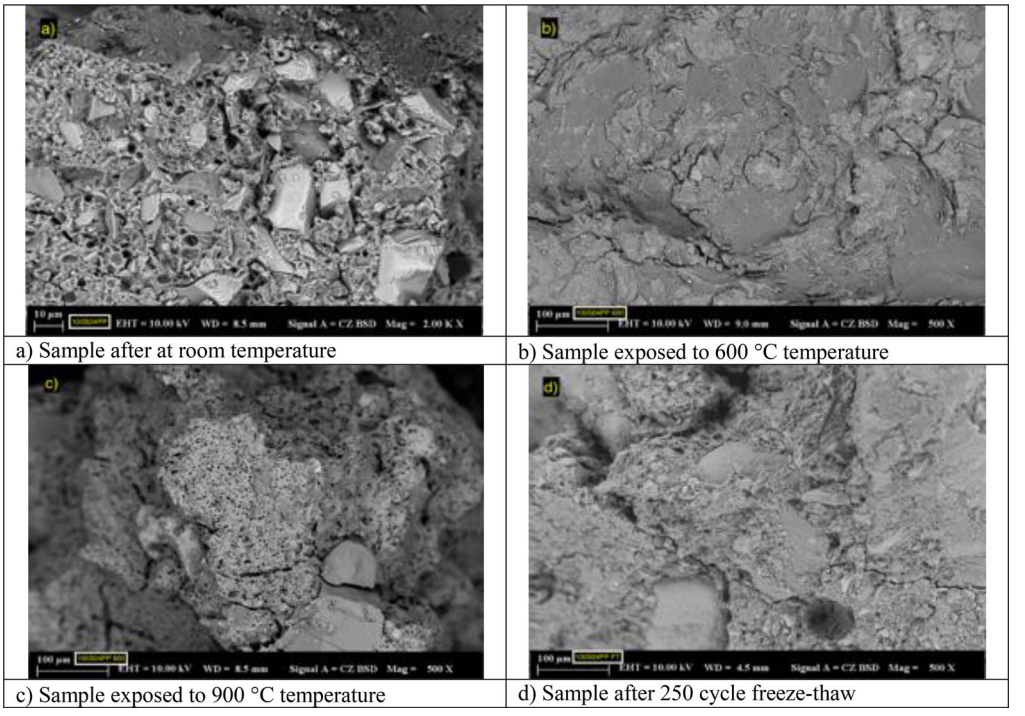

a) Sample after at room temperature | b) Sample exposed to 600 °C temperature

c) Sample exposed to 900 °C temperature | d) Sample after 250 cycle freeze-thaw

Figure 25. SEM micrographs of AASC samples reinforced with PP fibers.

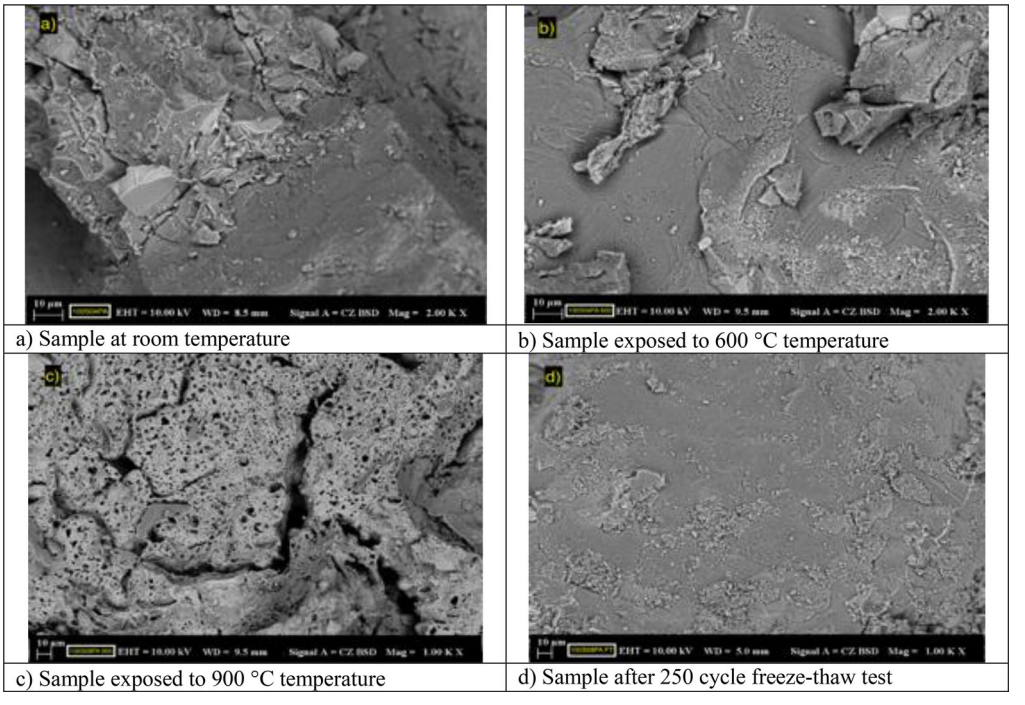

a) Sample at room temperature | b) Sample exposed to 600 °C temperature

c) Sample exposed to 900 °C temperature | d) Sample after 250 cycle freeze-thaw test

Figure 26. SEM micrographs of AASC samples reinforced with PA fibers.

The porous structure was seen in all mixture classes at 900°C. The microstructure of GGBS based AACs became more porous when exposed to high temperatures after 600°C due to matrix decomposition and weight loss. The porous structure was seen in all mixture classes at 900°C.

4. Conclusions

In this paper, research has been conducted to examine the effect of adding three different fibers on the mechanical and durability behavior of slag-based alkali-activated concretes and the conclusions are as follows:

- When the effect of fibers on compressive, splitting tensile, and flexural strength results were examined, it was observed that a decreasing trend occurred. This situation can be explained by the low bonding strength of the PP and PA fibered series at matrix interface transitions. Despite this situation, it was observed that steel fibers increased the splitting tensile strength. The addition of steel fibers to the AAS matrix effectively improved the post-crack behavior and positively affected the tensile strength.
- When the load-displacement curves and flexural toughness factor were examined, it was observed that PP and ST fibers significantly improved the post-crack behavior of alkali-activated concrete compared to the control sample. While it was observed that PA fibers improved flexural toughness factor values, it was found that it did not have a positive contribution to post-crack behavior.
- At 600 °C, the samples were exposed to a loss of strength between 8.8% and 38.96%, and at 900 °C, the samples were exposed to a loss of strength between 64.62% and 90.91% in terms of compressive strength.
- Apart from the PA fibered series, it can be said that the fiber addition did not have a positive effect on the flexural strength results after the freeze-thaw test. The PA fibered series showed complete improvement compared to the control series.
- The splitting tensile strengths of AASC were not close to those predicted by the ACI building code 318. An equation has been proposed that can accurately estimate the relationship between the splitting tensile strength and the corresponding compressive strength of AASC's. Estimated compressive strengths obtained at 600 °C, all the proposed models showed much more consistent results than the estimated compressive strengths obtained at 300 and 900 °C. In general, the Eurocode model gave closer results than other recommended models.

Funding

This work was supported by the research fund of the Yildiz Technical University, the authors would like to express their sincere gratitude to scientific research coordination unit for their financial support to the project (Project number: FBA-2019-3558).

ORCID

Ömer Faruk Kuranlı http://orcid.org/0000-0002-2937-1134
Mucteba Uysal http://orcid.org/0000-0002-6827-9904
Turgay Çoşgun http://orcid.org/0000-0002-5744-2040
Anıl Niş http://orcid.org/0000-0001-9092-8088
Yurdakul Aygörmez http://orcid.org/0000-0001-7405-2450
Orhan Canpolat http://orcid.org/0000-0003-2744-7876
Mukhallad M. Al-mashhadani http://orcid.org/0000-0002-1646-5879

References

ACI Committee 363. (1997). State-of-the-art report on high- strength concrete. *ACI 363R-92*. American Concrete Institute.

ACI Committee. (2005). *Building code requirements for structural concrete (ACI 318–05) and commentary (ACI 318R–05)*. American Concrete Institute.

Adesina, A. (2020). Performance of fibre reinforced alkali-activated composites – a review. *Materialia*, *12*, 100782. https://doi.org/10.1016/j.mtla.2020.100782

Aliabdo, A. A., Abd Elmoaty, A. E. M., & Emam, M. A. (2019). Factors affecting the mechanical properties of alkali activated ground granulated blast furnace slag concrete. *Construction and Building Materials.*, *197*, 339–355. https://doi.org/10.1016/j.conbuildmat.2018.11.086

Al-Majidi, M. H., Lampropoulos, A., & Cundy, A. B. (2017). Steel fibre reinforced geopolymer concrete (SFRGC) with improved microstructure and enhanced fibre-matrix interfacial properties. *Construction and Building Materials.*, *139*, 286–307. https://doi.org/10.1016/j.conbuildmat.2017.02.045

Al-Mashhadani, M. M., Canpolat, O., Aygörmez, Y., Uysal, M., & Erdem, S. (2018). Mechanical and microstructural characterization of fiber reinforced fly ash based geopolymer composites. *Construction and Building Materials.*, *167*, 505–513. https://doi.org/10.1016/j.conbuildmat.2018.02.061

Amran, M., Fediuk, R., Abdelgader, H. S., Murali, G., Ozbakkaloglu, T., Huei Lee, Y., & Lee, Y. Y. (2022). Fiber-reinforced alkali-activated concrete: A review. *Journal of Building Engineering*, *45*, 103638. Volume ISSN 2352-7102,. https://doi.org/10.1016/j.jobe.2021.103638

Aslani, F., & Samali, B. (2014). Constitutive relationships for steel fibre reinforced concrete at elevated temperatures. *Fire Technology*, *50*(5), 1249–1268. https://doi.org/10.1007/s10694-012-0322-5

ASTM C1609. (2019). *Standard test method for flexural performance of fiber-reinforced concrete (using beam with third-point loading)*. ASTM International.

ASTM C20-00. (2015). *Standard test methods for apparent porosity, water absorption, apparent specific gravity, and bulk density of burned refractory brick and shapes by boiling water*. ASTM International.

ASTM C597. (2016). *Standard test method for pulse velocity through concrete*. ASTM International.

Awoyera, P., & Adesina, A. (2020). Durability properties of alkali activated slag composites: Short overview. *Silicon*, *12*(4), 987–996. https://doi.org/10.1007/s12633-019-00199-1

Aygörmez, Y., Canpolat, O., Al-Mashhadani, M. M., & Uysal, M. (2020). Elevated temperature, freezing-thawing and wetting-drying effects on polypropylene fiber reinforced metakaolin based geopolymer composites. *Construction and Building Materials*, *235*, 117502. https://doi.org/10.1016/j.conbuildmat.2019.117502

Bhutta, A., Borges, P. H. R., Zanotti, C., Farooq, M., & Banthia, N. (2017). Flexural behavior of geopolymer composites reinforced with steel and polypropylene macro fibers. *Cement and Concrete Composites*, *80*, 31–40. https://doi.org/10.1016/j.cemconcomp.2016.11.014

Celik, A., Yilmaz, K., Canpolat, O., Al-Mashhadani, M. M., Aygörmez, Y., & Uysal, M. (2018). High-temperature behavior and mechanical characteristics of boron waste additive metakaolin based geopolymer composites reinforced with synthetic fibers. *Construction and Building Materials*, *187*, 1190–1203. https://doi.org/10.1016/j.conbuildmat.2018.08.062

Chi, M. (2012). Effects of dosage of alkali-activated solution and curing conditions on the properties and durability of alkali-activated slag concrete. *Construction and Building Materials*, *35*, 240–245. https://doi.org/10.1016/j.conbuildmat.2012.04.005

Ding, Y., Dai, J. G., & Shi, C. J. (2016). Mechanical properties of alkali-activated concrete: A state-of-the-art review. *Construction and Building Materials*, *127*, 68–79. https://doi.org/10.1016/j.conbuildmat.2016.09.121

Duxson, P., & Provis, J. L. (2008). Designing precursors for geopolymer cements. *Journal of the American Ceramic Society*, *91*(12), 3864–3869. https://doi.org/10.1111/j.1551-2916.2008.02787.x

El-Hassan, H., & Elkholy, S. (2021). Enhancing the performance of alkali-activated slag-fly ash blended concrete through hybrid steel fiber reinforcement. *Construction and Building Materials*, *311*, 125313. Volume . https://doi.org/10.1016/j.conbuildmat.2021.125313

El-Sayed, H. A., El-Enein, S. A. A., Khate, H. M., & Hasanein, S. A. (2011). Resistance of alkali activated water-cooled slaggeopolymer to sulphate attack. *Ceramic – Silikaty*, *55*, 153–160.

Eurocode. (2015). EN 1994-1-2. Design of composite steel and concrete structures – part 1–2: general rules – structural fire design.

Fan, F., Liu, Z., Xu, G., Peng, H., & Cai, C. S. (2018). Mechanical and thermal properties of fly ash based geopolymers. *Construction and Building Materials*, *160*, 66–81. https://doi.org/10.1016/j.conbuildmat.2017.11.023

Farhan, N. A., Sheikh, M. N., & Hadi, M. N. S. (2018). Engineering properties of ambient cured alkali-activated fly ash-slag concrete reinforced with different types of steel fiber. *Journal of Materials in Civil Engineering*, *30*(7), 04018142. https://doi.org/10.1061/(ASCE)MT.1943-5533.0002333

Guerrieri, M., Sanjayan, J., & Collins, F. (2009). Residual compressive behavior of alkali-activated concrete exposed to elevated temperatures. *Fire and Materials*, *33*(1), 51–62. https://doi.org/10.1002/fam.983

Hardjito, D., Wallah, S. E., Sumajouw, D. M. J., & Rangan, B. V. (2004). Factors influencing the compressive strength of fly ash-based geopolymer concrete. *Civil Engineering*, *6*, 88–93. http://www.freepatentsonline.com/article/Civil-Engineering-Dimension/170455954.html.

Hossain, M. Z., Shahjalal, M., Islam, K., Tiznobaik, M., & Alam, M. S. (2019). Mechanical properties of recycled aggregate concrete containing crumb rubber and polypropylene fiber. *Construction and Building Materials*, *225*, 983–996. https://doi.org/10.1016/j.conbuildmat.2019.07.245

Hussin, M. W., Bhutta, M. A. R., Azreen, M., Ramadhansyah, P. J., & Mirza, J. (2015). Performance of blended ash geopolymer concrete at elevated temperatures. *Materials and Structures*, *48*(3), 709–720. https://doi.org/10.1617/s11527-014-0251-5

IS 456-2000. Code of practice for plain and reinforced cement concrete.

Japan Society of Civil Engineers JSCE-SF4 (1984). Method of test for flexural strength and flexural toughness of steel fibre reinforced concrete. *Concrete Library International*, Part III-2, No. 3, 58–61.

Kalifa, P., Chéné, G., & Gallé, C. (2001). High-temperature behaviour of HPC with polypropylene fibres. *Cement and Concrete Research*., *31*(10), 1487–1499. https://doi.org/10.1016/S0008-8846(01)00596-8

Kampala, A., Horpibulsuk, S., Prongmanee, N., & Chinkulkijniwat, A. (2014). Influence of wet-dry cycles on compressive strength of calcium carbide residue – fly ash stabilized clay. *Journal of Materials in Civil Engineering*, *26*(4), 633–643. https://doi.org/10.1061/(ASCE)MT.1943-5533.0000853

Khalaj, M. J., Khoshakhlagh, A., Bahri, S., Khoeini, M., & Nazerfakhari, M. (2015). Split tensile strength of slag-based geopolymer composites reinforced with steel fibers: Application of Taguchi method in evaluating the effect of production parameters and their optimum condition. *Ceramics International*, *41*(9), 10697–10701. https://doi.org/10.1016/j.ceramint.2015.05.002

Koenig, A., Wuestemann, A., Gatti, F., Rossi, L., Fuchs, F., Fessel, D., Dathe, F., Dehn, F., & Minelli, F. (2019). Flexural behaviour of steel and macro-PP fibre reinforced concretes based on alkali-activated binders. *Construction and Building Materials*, *211*, 583–593. https://doi.org/10.1016/j.conbuildmat.2019.03.227

Kong, D. L. Y., Sanjayan, J. G., & Sagoe-Crentsil, K. (2008). K. Sagoe-Crentsil, Factors affecting the performance of metakaolin geopolymers exposed to elevated temperatures. *Journal of Materials Science*, *43*(3), 824–831. https://doi.org/10.1007/s10853-007-2205-6

Malhotra, V. M., & Mehta, P. K. (2002). High-performance, high-volume fly ash concrete: Materials, mixture proportioning, properties, construction practice, and case histories. *Canada: N*, p., Web.

Md. Nabi, N. K., & Sarker, P. K. (2020). Effect of waste glass fine aggregate on the strength, durability and high temperature resistance of alkali-activated fly ash and GGBFS blended mortar. *Construction and Building Materials*, *263*, 120177. https://doi.org/10.1016/j.conbuildmat.2020.120177.

Mustafa, M., Bakri, A., Mohammed, H., Kamarudin, H., Niza, I. K., & Zarina, Y. (2011). Review on fly ash-based geopolymer concrete without Portland Cement. *Journal of Engineering and Technology Research*, *3*, 1–4.

Noushini, A., Hastings, M., Castel, A., & Aslani, F. (2018). Mechanical and flexural performance of synthetic fibre reinforced geopolymer concrete. *Construction and Building Materials*, *186*, 454–475. https://doi.org/10.1016/j.conbuildmat.2018.07.110

Parthiban, K., & Mohan, K. S. R. (2017). Influence of recycled concrete aggregates on the engineering and durability properties of alkali activated slag concrete. *Construction and Building Materials*, *133*, 65–72. https://doi.org/10.1016/j.conbuildmat.2016.12.050

Provis, J. L. (2018). Alkali-activated materials. *Cement and Concrete Research*, *114*, 40–48. https://doi.org/10.1016/j.cemconres.2017.02.009

Pu, X. C., Gan, C. C., Wang, S. D., & Yang, C. H. (1988). Summary reports of research on alkali-activated slag cement and concrete. *Chongqing Institute of Architectural Engineering of Chongqing*, *1*, 6.

Puertas, F., Amat, T., Fernández-Jiménez, A., & Vázquez, T. (2003). Mechanical and durable behaviour of alkaline cement mortars reinforced with polypropylene fibres. *Cement and Concrete Research*, *33*(12), 2031–2036. https://doi.org/10.1016/S0008-8846(03)00222-9

Qu, F., Li, W., Tao, Z., Castel, A., & Wang, K. (2020). High temperature resistance of fly ash/GGBFS-based geopolymer mortar with load-induced damage. *Materials and Structures*, *53*(4), 111. https://doi.org/10.1617/s11527-020-01544-2

Rao, G. M., Rao, T. G., Reddy, M. S. N., & Seshu, D. R. (2019). A study on the strength and performance of geopolymer concrete subjected to elevated temperatures. *Recent Advances in Structural Engineering*, *1*, 869–889.

Rovnanik, P., Bayer, P., & Rovnanikova, P. (2013). Characterization of alkali activated slag paste after exposure to high temperatures. *Construction and Building Materials*, *47*, 1479–1487. https://doi.org/10.1016/j.conbuildmat.2013.06.070

Shaikh, F. U. A. (2013). Review of mechanical properties of short fibre reinforced geopolymer composites. *Construction and Building Materials*, *43*, 37–49. https://doi.org/10.1016/j.conbuildmat.2013.01.026

Shaikh, F. U. A., & Hosan, A. (2016). Mechanical properties of steel fibre reinforced geopolymer concretes at elevated temperatures. *Construction and Building Materials*, *114*, 15–28. https://doi.org/10.1016/j.conbuildmat.2016.03.158

Shehab, H. K., Eisa, A. S., & Wahba, A. M. (2016). Mechanical properties of fly ash based geopolymer concrete with full and partial cement replacement. *Construction and Building Materials*, *126*, 560–565. https://doi.org/10.1016/j.conbuildmat.2016.09.059

Sun, P., & Wu, H. C. (2013). Chemical and freeze-thaw resistance of fly ash-based inorganic mortars. *Fuel*, *111*, 740–745. https://doi.org/10.1016/j.fuel.2013.04.070

Timothy, A. A. J., Kwasny, W., Sha, K. T. & Tong, (2021). Mechanical and durability properties of alkali-activated fly ash concrete with increasing slag content. *Construction and Building Materials*, *301*, 124330. https://doi.org/10.1016/j.conbuildmat.2021.124330.

Turkey, F. A., Beddu, S. B., Ahmed, A. N., & Al-Hubboubi, S. (2021). A review – behaviour of geopolymer concrete to high temperature. Materials Today: *Proceedings*. https://doi.org/10.1016/j.matpr.2021.05.489.

Xu, F., Deng, X., Peng, C., Zhu, J., & Chen, J. (2017). Mix design and flexural toughness of PVA fiber reinforced fly ash-geopolymer composites. *Construction and Building Materials*, *150*, 179–189. https://doi.org/10.1016/j.conbuildmat.2017.05.172

Yang, K. H., Cho, A. R., & Song, J. K. (2012). Effect of water-binder ratio on the mechanical properties of calcium hydroxide-based alkali-activated slag concrete. *Construction and Building Materials*, *29*, 504–511. https://doi.org/10.1016/j.conbuildmat.2011.10.062

Yurt, Ü. (2020). An experimental study on fracture energy of alkali activated slag composites incorporated different fibers. *Journal of Building Engineering*, *32*, 101519. https://doi.org/10.1016/j.jobe.2020.101519

Zhang, H., Li, L., Yuan, C., Wang, Q., Kumar Sarker, P., & Shi, X. (2020). Deterioration of ambient-cured and heat-cured fly ash geopolymer concrete by high temperature exposure and prediction of its residual compressive strength. *Construction and Building Materials*, *262*, 120924. Volume . https://doi.org/10.1016/j.conbuildmat.2020.120924

Zhou, X., Zeng, Y., Chen, P., Jiao, Z., & Zheng, W. (2021). Mechanical properties of basalt and polypropylene fibre-reinforced alkali-activated slag concrete. *Construction and Building Materials*, *269*, 121284. https://doi.org/10.1016/j.conbuildmat.2020.121284